Electronic Supplementary Material (ESI) for ChemComm.

Morphological Tuning and Control of Self-Assembled Multivalent (SAMul) Heparin Binding in Highly Competitive Media

Ana C. Rodrigo,[a] Stephen M. Bromfield,[a] Erik Laurini,[b] Paola Posocco,[b] Sabrina Pricl[b] and David K. Smith[a,*]

a: Department of Chemistry, University of York, Heslington, York, YO10 5DD, UK

b: Molecular Simulation Engineering (MOSE) Laboratory, Department of Engineering and Architecture, University of Trieste, Piazzale Europa 1, 34127 Trieste, Italy and National Interuniversity Consortium for Material Science and Technology (INSTM), Research Unit MOSE-DEA, University of Trieste, Piazzale Europa 1, 32127 Trieste, Italy

1 General Experimental Methods.

All compounds required in synthesis and analysis were purchased from standard commercial suppliers. Proton and carbon NMR spectra were recorded on a Jeol 400 spectrometer (^{1}H 400 MHz, ^{13}C 100 MHz). Samples were recorded as solutions in deuterated NMR solvents as stated and chemical shifts (δ) are quoted in parts per million. Coupling constant values (*J*) are given in Hz. The level of assignment of ^{1}H NMR spectra was achieved using model compounds, literature data and standard knowledge of ^{1}H NMR. DEPT experiments were used to assist in the assignment of ^{13}C NMR spectra. Positive and negative ion electrospray mass spectra were recorded on a Bruker Daltonics MicroTOF mass spectrometer. IR spectra were recorded on a PerkinElmer Spectrum Two FT-IR spectrometer. Melting points were measured on a Stuart SMP3 melting point apparatus and are uncorrected. UV-vis absorbance was measured on a Shimadzu UV-2401 PC spectrophotometer. Fluorescence was measured on a Hitachi F-4500 spectrofluorimeter. CD spectra were recorded on a Jasco J810 CD Spectrophotometer (150 W Xe lamp).

2 Synthetic Methods

Boc-protected amino acids were synthesised using standard Boc-protection methods. All other reagents and solvents were provided by chemical suppliers. All procedures used to synthesise D-enantiomers were identical to those for L-enantiomers – all data were identical except for α_D values and CD spectra (see Section 2), which were mirror images of one another.

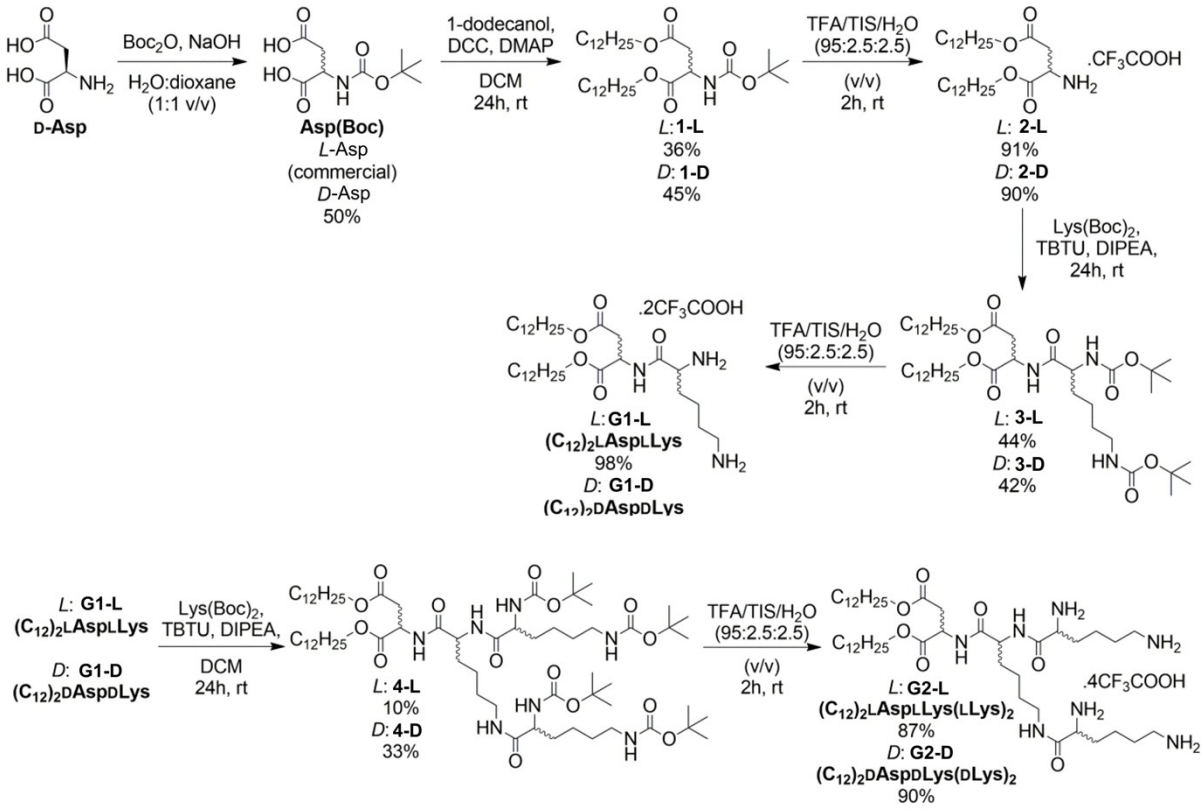

Scheme S1. Synthesis of Self-Assembling Multivalent (SAMul) ligands **G1** and **G2**.

Synthesis of $(C_{12})_2$-L-Asp-Boc (1-L and 1-D). Boc-L-Asp-$(OH)_2$ (1.00 g, 4.28 mmol, 1 eq.), 1-dodecanol (3.20 g, 17.2 mmol, 4 eq.), DCC (1.77 g, 8.58 mmol, 2 eq.) and DMAP (1.05 g, 8.58 mmol, 2 eq.) were dissolved together in anhydrous DCM (50 mL). The stirred mixture was kept for 10 minutes at 0°C before being allowed to warm to room temperature and left overnight under an N_2 atmosphere. The DCU by-product was removed by filtration through a Celite-containing sinter funnel and the filtrate concentrated to a residue *in vacuo*. This residue was taken up in DCM (60 mL) and washed successively with HCl (2 × 30 mL, 0.5 M) and $NaHCO_3$ (30 mL, sat.). The organic phase was collected, dried over $MgSO_4$ and the resulting filtrate concentrated *in vacuo* to afford a clear yellow residue. Purification by flash column chromatography (SiO_2, 95 : 5, DCM : ethyl acetate) afforded pure product as a white powdery solid (**1-L**: 877 mg, 1.54 mmol, 36%; **1-D** yield: 45%). R_f = 0.95 (9:1 DCM:methanol, ninhydrin). ^{1}H NMR (400 MHz, $CDCl_3$) δ: 5.49 (d, N*H*, 1H); 4.52 (exp dd, app t, C*H*NH, ^{3}J = 4.4 Hz, 1H); 4.18-4.10 (exp t, app m, CH_2OC(O)CH_2, 2H); 4.05 (t, CH_2OC(O)CH, ^{3}J = 6.8 Hz, 2H); 2.99 (dd, CH_aH$_b$CHNH, ^{2}J^{3}J = 17.2 Hz, 4.4 Hz, 1H); 2.77 (dd, CH$_a$$H_b$CHNH, ^{2}J^{3}J = 17.2 Hz, 4.4 Hz, 1H); 1.65-1.59 (m, CH_2CH$_2$O, 4H); 1.44 (s, C(CH_3)$_3$, 9H); 1.23 (br s, 18 × alkylCH_2, 36H); 0.88 (t, 2 × alkylCH_3, ^{3}J = 6.4 Hz, 6H). ^{13}C NMR (100 MHz, $CDCl_3$) δ: 171.14, 171.03 (*C*=O, ester); 155.43 (*C*=O, carbamate); 80.00 (*C*(CH$_3$)$_3$); 65.88, 65.19 (*C*H$_2$O); 49.84

(*C*HNH); 36.80 (C*H*$_2$CHNH); 31.90, 29.62, 29.57, 29.51, 29.34, 29.23, 28.50, 28.45, 28.28 (alkyl*C*H$_2$); 25.84, 25.79 (*C*H$_2$CH$_2$O); 22.67 (C(*C*H$_3$)$_3$); 14.11 (alkyl*C*H$_3$). ESI-MS: 592.45 [M+Na]$^+$ (100%), 570.47 [M+H]$^+$ (44%). HRMS: Calcd. [M+Na]$^+$ ($C_{33}H_{63}NNaO_6$) *m/z* = 592.4548, found [M+Na]$^+$ *m/z* = 592.4520 (error 3.9 ppm). IR ν [cm^{-1}]: 3403*w* (N–H stretch), 2955*w*, 2918*s* (C–H), 2851*m* (C–H), 1733*s* (C=O, esters), 1709*s* (CONH, carbamate I), 1506*m* (CONH, carbamate II), 1467*m*, 1456*w*, 1420*w*, 1393*w* (C–H), 1342*m*, 1209*m*, 1165*s* (C–N stretch), 1073*w*, 1055*w*, 1041*w*, 781*w*, 721*m*. θ_L: + 33.6 mdeg (223 nm, 10 mM, MeOH); θ_D: − 25.0 mdeg (223 nm, 10 mM, MeOH).

Synthesis of $(C_{12})_2$-L-Asp.TFA (2-L and 2-D). $(C_{12})_2$-L-Asp-Boc (**1-L**, 200 mg, 3.51 mmol, or **1-D**) was dissolved in a mixture of trifluoroacetic acid, triisopropylsilane and deionised water (500 μL, 95 : 2.5 : 2.5 v/v) before being shaken until TLC indicated reaction to be complete (3.5 h). Following careful addition of deionised water (1.5 mL), the reaction mixture was washed with chloroform (3 × 4 mL) to extract non polar by-products. The aqueous layer was then evaporated to dryness in vacuo to afford the product as a white powdery solid (**2-L**: 186 mg, 3.19 mmol, 91%; **2-D** yield: 90%). R_f = 0.76 (9:1 DCM:methanol, ninhydrin). ^{1}H NMR (400 MHz, $CDCl_3$) δ: 4.36 (exp dd, app t, C*H*NH$_3^+$, ^{3}J = 4.8 Hz, 1H); 4.26-4.15 (exp t, app m, C*H*$_2$OC(O)CH$_2$, 2H); 4.10 (t, C*H*$_2$OC(O)CH, ^{3}J = 6.8 Hz, 2H); 3.12 (d, C*H*$_2$CHNH, ^{3}J = 4.8 Hz, 2H); 1.65-1.58 (m, C*H*$_2$CH$_2$O, 4H); 1.25 (br s, 18 × alkylC*H*$_2$, 36H); 0.88 (t, 2 × alkylC*H*$_3$, ^{3}J = 6.8 Hz, 6H). ^{13}C NMR (100 MHz, $CDCl_3$) δ: 171.74, 167.92 (*C*=O, ester); 161.60 (*C*=O, acid); 67.57, 66.39 (*C*H$_2$O); 49.73 (*C*HNH); 33.13 (*C*H$_2$CHNH); 31.91, 29.65, 29.62, 29.58, 29.49, 29.47, 29.34, 29.22, 29.15, 28.28, 28.17, 25.72, 25.59 (alkyl*C*H$_2$); 14.11 (alkyl*C*H$_3$). ESI-MS: 470.42 [M–TFA+H]$^+$ (100%). HRMS: Calcd. [M+H]$^+$ ($C_{28}H_{56}NO_4$) *m/z* = 470.4204, found [M+H]$^+$ = 470.4190 (error 2.5 ppm). IR ν [cm^{-1}]: 2955*w*, 2918*s* (N–H), 2850*m* (C–H), 1752*m* (C=O, ester), 1736*m* (C=O, acid) 1665*s*, 1593*w*, 1466*w*, 1431*w*, 1399*w*, 1371*w* (C–H), 1245*m* (C–O), 1186*s* (C–N), 1141*m*, 1125*m*, 1092*w*, 803*m*, 766*w*. θ_L: + 26.7 mdeg (210 nm, 10 mM, MeOH); θ_D: − 27.6 mdeg (210 nm, 10 mM, MeOH).

Synthesis of $(C_{12})_2$-L-Asp-L-Lys(Boc)$_2$ (3-L and 3-D). L-Lys(Boc)$_2$ (76 mg, 0.22 mmol, 1.1 eq., or D-Lys(Boc)$_2$) was dissolved in DCM (13 mL) at 0°C and stirred for 10 min before TBTU (63 mg, 0.20 mmol, 1 eq.) was added. After a further 10 minutes, $(C_{12})_2$-L-Asp.TFA (**2-L**, 100 mg, 0.21 mmol, 1 eq., pre-dissolved in DCM (4 mL), or **2-D**) and DIPEA (52 mg, 0.40 mmol, 2 eq.) were added. The resulting reaction mixture was stirred at 0°C for 20 minutes before being warmed to room temperature and left to stir overnight. The volatiles were *removed in*

vacuo and the resulting residue taken up in DCM (10 mL) and washed successively with $NaHSO_4$ (2 × 15 mL, 1.33 M), $NaHCO_3$ (2 × 10 mL, sat.), deionised water (3 × 15 mL) and brine (15 mL, sat.). The organic phase was collected, dried over $MgSO_4$ and the resulting filtrate concentrated *in vacuo* to afford a white powdery solid, which was purified by flash column chromatography (SiO_2, 1:1 cyclohexane:ethyl acetate) to afford the product as a white powdery solid (**3-L**: 75 mg, 94 μmol, 44%; **3-D** yield: 42%). R_f = 0.85 (9:1 DCM:methanol, ninhydrin). ^{1}H NMR (400 MHz, $CDCl_3$) δ: 6.89 (d, AspN*H*, ^{3}J = 8.0 Hz, 1H); 5.16 (br s, LysCH$_2$N*H*, 1H); 4.81 (exp dd, app dt, AspC*H*NH, ^{3}J^{3}J = 8.0 Hz, 4.4 Hz, 1H); 4.67 (exp dd, app br s, LysC*H*NH, 1H); 4.17-4.06 (exp dd, app m, LysC*H*NH, 2 × CH_2O, 5H); 3.11 (exp t, app s, CH_2NH, 2H); 3.02 (dd, CH_aH$_b$CHNHAsp, ^{2}J^{3}J = 17.2 Hz, 4.4 Hz, 1H); 2.80 (dd, CH$_a$$H_b$CHNHAsp, ^{2}J^{3}J = 17.2 Hz, 4.4 Hz, 1H); 1.81-1.71 (m, CH_2CH$_2$NH, 2H); 1.67-1.58 (m, 2 × CH_2CH$_2$O, LysCH_2CHNH, 6H); 1.43 (s, (CH_3)$_3$, 18H); 1.25 (s, 18 × alkylCH_2, CH_2CH$_2$CHNH, 38H); 0.87 (t, 2 × alkylCH_3, ^{3}J = 7.2 Hz, 6H). ^{13}C NMR (100 MHz, $CDCl_3$) δ: 171.78, 170.97 (*C*=O, ester); 170.44 (*C*=O, amide); 156.08 (2 × *C*=O, carbamate); 79.94, 79.93 (*C*(CH$_3$)$_3$); 66.03, 65.31 (*C*H$_2$O); 48.45 (Asp*C*HNH); 36.17 (Asp*C*H$_2$CHNH); 31.88 (*C*H$_2$CH$_2$NH); 29.62, 29.60, 29.56, 29.50 29.32, 29.23, 29.19 (alkyl*C*H$_2$); 28.34, 28.21 (C(*C*H$_3$)$_3$); 25.76, 25.68 (alkyl*C*H$_2$); 22.59 (Lys*C*H$_2$CHNH); 14.02 (2 × alkyl*C*H$_3$). ESI-MS: 820.60 [M+Na]$^+$ (100%). HRMS: Calcd. [M+Na]$^+$ ($C_{44}H_{83}N_3NaO_9$) *m/z* = 820.6022, found [M+Na]$^+$ = 820.5995 (error 2.8 ppm). IR ν [cm^{-1}]: 3356*w* (N–H), 3331*w* (N–H), 2918*s* (C–H), 2850*m* (C–H), 1746*m* (C=O, ester), 1730*m* (C=O, ester), 1682*s* (CONH, amide I), 1656*s* (CONH, carbamates I), 1528*s* (CONH, amide II), 1471*w*, 1403*w*, 1392*w*, 1365*w*, 1301*m*, 1275*m*, 1247*m* (C–O), 1170*s* (C–N), 1087*w*, 1053*w*, 1019*w*, 783*w*, 766*w*, 732*w*, 719*w*. **3-L** α_D: +13.5 (c. 1.0, $CHCl_3$). **3-D** α_D: −11.2 (c. 1.0, $CHCl_3$).

Synthesis of (C$_{12}$)$_2$-L-Asp-L-Lys.2TFA (G1-L and G1-D). (C$_{12}$)$_2$-L-Asp-L-Lys(Boc)$_2$ (**3-L**, 49 mg, 61 μmol, or **3-D**) was dissolved in a mixture of trifluoroacetic acid, triisopropylsilane and deionised water (500 μL, 95 : 2.5 : 2.5 v/v) before being shaken until TLC indicated reaction to be complete (2.5 h). Following careful addition of deionised water (1.5 mL), the reaction mixture was washed with chloroform (3 × 4 mL). The combined organic layers were dried over $MgSO_4$ and resulting filtrate concentrated *in vacuo* to afford the product as a white powdery solid (**G1-L**: 36 mg, 60 μmol, 98%; **G1-D** yield: 97%). R_f = 0.07 (9:1 DCM:methanol, ninhydrin). ^{1}H NMR (400 MHz, $CDCl_3$) δ: 7.82-7.75 (br m, CHNH_3^+, 3H); 7.34 (s, CH$_2$NH_3^+, 2H); 4.89-4.84 (exp dd, app m, AspC*H*NH, 1H); 4.20 (br s, AspCHN*H*, 1H); 4.16-4.07 (exp dd, app m, C*H*NH$_3^+$, 1H); 4.07-4.00 (m, 2 × CH_2O, 4H); 3.08 (exp t, app s, CH_2NH$_3^+$, 2H); 2.97 (dd, CH_aH$_b$CHNHAsp, ^{2}J^{3}J = 17.4 Hz, 5.6 Hz, 1H); 2.80 (dd, CH$_a$$H_b$CHNHAsp, ^{2}J^{3}J =

17.4 Hz, 3.2 Hz, 1H); 1.96 (br s, CH_2CHNH$_3^+$, 2H); 1.74 (s, CH_2CH$_2$NH$_3^+$, 2H); 1.58 (br s, 2 × CH_2CH$_2$O, CH_2CH$_2$CHNH$_3^+$, 6H); 1.25 (s, 18 × alkylCH_2, 36H); 0.88 (t, 2 × alkylCH_3, ^{3}J = 6.8 Hz, 6H). ^{13}C NMR (100 MHz, $CDCl_3$) δ: 171.80, 171.16 (*C*=O, esters); 170.51 (*C*=O, amide); 161.04 (*C*=O, acid); 66.86, 66.11 (*C*H$_2$O); 61.09 (*C*HNH$_3^+$); 60.51 (*C*H$_2$NH$_3^+$); 48.10 (*C*HNHAsp); 39.61 (*C*H$_2$CHNH$_3^+$); 34.00 (Asp*C*H$_2$CHNH); 31.89, 29.64, 29.62, 29.58, 29.49, 29.34, 29.24, 29.18, 28.24 (alkyl*C*H$_2$); 28.20 (*C*H$_2$CH$_2$NH$_3^+$); 25.71, 25.66 (alkyl*C*H$_2$); 14.04 (2 × alkyl*C*H$_3$). ESI-MS: 598.51 [M+H]$^+$ (100%). HRMS: Calcd. [M+H]$^+$ ($C_{34}H_{68}N_3O_5$) *m/z* = 598.5153, found [M+H]$^+$ = 598.5139 (error 2.6 ppm). IR ν [cm^{-1}]: 3330*w* (N–H), 2917*s* (C–H), 2850*m* (C–H), 1751*m* (C=O, ester), 1725*m* (C=O, ester), 1668*s* (CONH, amide I), 1539*m* (CONH, amide II), 1469*w*, 1430*w*, 1417*w*, 1401*w*, 1362*w* (C–H), 1345*w*, 1303*w*, 1271*w*, 1201*s* (C–O), 1178*s* (C–N), 1128*s*, 1078*w*, 1064*w*, 1003*w*, 739*w*, 721*s*. θ_L: + 94.4 mdeg (215 nm, 10 mM, MeOH). θ_D: − 105.3 mdeg (215 nm, 10 mM, MeOH).

Synthesis of $(C_{12})_2$-L-Asp-L-Lys(L-Lys(Boc)2)2 (4-L and 4-D). L-Lys(Boc)$_2$ (185 mg, 530 μmol, 2.2 eq, or D-Lys(Boc)$_2$) was dissolved in DCM (10 mL) at 0°C and TBTU (171 mg, 530 μmol, 2.2 eq) was added. After stirring for 10 min, $(C_{12})_2$-L-Asp-L-Lys.TFA (**G1-L**, 200 mg, 240 μmol, 1 eq., or **G1-D**) and DIPEA (169 μL, 970 μmol, 4 eq) were added along with more cold DCM (10 mL). After 20 min, the reaction mixture was allowed to warm to room temperature, and stirred for 40 h. The volatiles were removed *in vacuo* and resulting residue taken up in DCM (20 mL) before being washed successively with $NaHSO_4$ (2 × 10 mL, 1.33 M), $NaHCO_3$ (2 × 10 mL, sat.), deionised water (3 × 10 mL) and brine (10 mL, sat.). The organic phase was collected, dried over $MgSO_4$ and the resulting filtrate concentrated *in vacuo* to afford a golden solid. This solid was purified by flash column chromatography (SiO2, 8:2, ethyl acetate:cyclohexane) to afford the product as a sticky white solid (**4-L**: 31 mg, 25 μmol, 10%; **4-D** yield: 33%. R_f= 0.69 (8:2 ethyl acetate:cyclohexane, ninhydrin). ^{1}H NMR (400 MHz, $CDCl_3$) δ: 7.09 (d, AspN*H*, J = 7.6 Hz, 1H); 6.92 (s, LysN*H*, 1H); 5.95 (s, LysN*H*, 1H); 5.50 (s, LysN*H*, 1H); 4.85-4.77 (exp dd, app m, AspC*H*NH, 1H); 4.29 (exp dd, br s, 2 × C*H*NHBoc, 2H); 4.13 – 3.95 (m, 2 × CH_2O, LysC*H*NHLys 5H); 3.10 (exp m, app s, 2 × CH_2NHBoc, CH_2NHLys, 6H); 3.01 (dd, AspCH_aH$_b$CHNH, ^{2}J^{3}J = 17.4 Hz, 4.6 Hz, 1H); 2.77 (dd, AspCH$_a$$H_b$CHNH, ^{2}J^{3}J = 17.4 Hz, 4.6 Hz, 1H); 1.77-1.70 (m, 2 × CH_2CHNHBoc, LysCH_2CHNHLys, 6H); 1.68-1.62 (m, 2 × CH_2CH$_2$O, 4H); 1.58-1.46 (m, 2 × CH_2CH$_2$NHBoc, LysCH_2CH$_2$NHLys, 6H); 1.42 (s, 2 × C(CH_3)$_3$, 3 × CH_2CH$_2$CHNH, 24H); 1.41 (s, C(CH_3)$_3$, 9H) 1.40 (s, C(CH_3)$_3$, 9H); 1.25 (app s, 18 × alkylCH_2, 36H); 0.87 (t, 2 × alkylCH_3, ^{3}J = 7.0 Hz, 6H). ^{13}C NMR (100 MHz, $CDCl_3$) δ: 173.41 (2 × *C*=O, ester); 171.02 (3 × *C*=O, amide);

156.12, 156.05 (2 × *C*=O, carbamate); 80.69, 79.81 (2 × *C*(CH_3)$_3$); 66.08, 65.33 (*C*H_2O); 54.42, 54.02 (*C*H_2NHBoc); 53.91, 53.86 (*C*HNHBoc); 48.41 (Asp*C*HNHLys); 40.33, 40.09, 40.03 (Lys*C*H_2CHNH); 36.18 (Asp*C*H_2CHNH); 31.88 (2 × *C*$H_2$$CH_2$NHBoc, *C*$H_2$$CH_2$NHLys); 29.64, 29.61, 29.52, 29.41, 29.33, 29.26, 29.28, 28.49 (alkyl*C*H_2); 28.43, 28.36 (2 × C(*C*H_3)$_3$); 25.86, 25.79 (alkyl*C*H_2); 22.66 (2 × *C*$H_2$$CH_2$CHNHBoc, *C*$H_2$$CH_2$CHNHLys); 14.09 (2 × alkyl*C*H_3). ESI-MS: 1276.89 $[M+Na]^+$ (100%). HRMS: Calcd. $[M+Na]^+$ ($C_{66}H_{123}N_7NaO_{15}$) *m/z* = 1276.8969, found $[M+Na]^+$ = 1276.8930 (error 3.0 ppm). IR ν [cm^{-1}]: 3301*m* (N–H), 2925*s* (C–H), 2855*m* (C–H), 1739*m* (C=O, esters), 1688*s* (CONH, amide I), 1644*s* (CONH, carbamates I), 1520*s* (CONH, amide II), 1456*m*, 1391*m*, 1365*s*, 1272*w*, 1247*s* (C–N), 1168*s* (C–N), 1091*w*, 1046*w*, 1017*w*, 867*w*, 782*w*. **4-L** α_D: + 18.4 (c. 1.0, $CHCl_3$). **4-D** α_D: − 22.2 (c. 1.0, $CHCl_3$).

Synthesis of $(C_{12})_2$-L-Asp-L-Lys(L-Lys)$_2$.4TFA (G2-L and G2-D)

(C12)2-L-Asp-L-Lys(L-Lys(Boc)$_2$)$_2$ (**4-L**, 28 mg, 22 μmol, or **4-D**) was dissolved in a mixture of trifluoroacetic acid, triisopropylsilane and deionised water (500 μL, 95 : 2.5 : 2.5 v/v) before being shaken until TLC indicated reaction to be complete (2 h). Following careful addition of deionised water (1.5 mL), the reaction mixture was washed with chloroform (3 × 4 mL). The combined organic layers were dried over $MgSO_4$ and the resulting filtrate concentrated *in vacuo* to afford the product as a white powdery solid (**G2-L**: 25 mg, 19 μmol, 87%; **G2-D** yield: 90%). R_f = 0.00 (9:1 DCM:methanol, ninhydrin). ^{1}H NMR (400 MHz, CD_3OD) δ: 4.82 (exp dd, app t, AspC*H*NH, ^{3}J = 6.4 Hz, 1H); 4.38 (exp dd, app t, LysC*H*NH, ^{3}J = 5.6 Hz, 1H); 4.19-4.05 (m, 2 × C*H*$_2$O, 4H); 3.95 (t, C*H*NH_3^+, ^{3}J = 5.4 Hz, 1H); 3.85 (t, C*H*NH_3^+, ^{3}J = 6.0 Hz, 1H); 3.29-3.18 (m, C*H*$_2$NH, 2H); 3.00-2.92 (m, 2 × C*H*$_2$$NH_3^+$, 4H); 2.87 (d, AspC*H*$_2$CHNH, ^{3}J = 6.4 Hz, 2H); 1.94 – 1.82 (m, 2 × C*H*$_2$$CHNH_3^+$, C*H*$_2$CHNH, 6H); 1.74-1.69 (m, 2 × C*H*$_2$$CH_2$$NH_3^+$, C*H*$_2$$CH_2$NH, 6H); 1.64 (exp m, app s, 2 × C*H*$_2$$CH_2$O, 4H); 1.52-1.43 (m, 2 × C*H*$_2$$CH_2$$CHNH_3^+$, C*H*$_2$$CH_2$CHNH, 6H); 1.30 (s, 18 × alkylC*H*$_2$, 36H); 0.90 (t, 2 × alkylC*H*$_3$, ^{3}J = 6.8 Hz, 6H). ^{13}C NMR (100 MHz, CD_3OD) δ: 173.87, 172.12 (*C*=O, esters); 172.05, 170.09, 170.00 (*C*=O, amide); 77.66 (2 × *C*$H_2$$NH_3^+$); 66.95, 66.42 (*C*$H_2$O); 54.87 (*C*$H_2$NH, Lys*C*HNHLys); 54.31, 53.93 (*C*HNH_3^+); 49.05 (Asp*C*HNH); 40.48, 40.30, 40.26 (Lys*C*H_2CHN); 37.03 (Asp*C*H_2CHNH); 33.14, 32.73, 32.17 (*C*$H_2$$CH_2$N); 30.82, 30.78, 30.55, 30.50, 30.47, 29.96, 29.74, 29.71, 27.12, 27.09 (alkyl*C*H_2); 23.80, 23.02, 22.41 (*C*$H_2$$CH_2$CHN); 14.50 (2 × alkyl*C*H_3). ESI-MS: 427.85 $[M+2H]^{2+}$ (100%), 854.71 $[M+H]^+$ (13%). HRMS: Calcd. $[M+2H]^{2+}$ ($C_{46}H_{93}N_7NaO_7$) *m/z* = 427.8563, found $[M+H]^+$ = 427.8545 (error 4.4 ppm). IR ν [cm^{-1}]: 3305*m* (N–H), 2930*s* (C–H), 2855*m* (C–H), 1739*m* (C=O, esters), 1689*s* (CONH, amide

I), 1524*s* (CONH, amide II), 1455*m*, 1390*m*, 1364*s*, 1248*s* (C–N), 1168*s* (C–N), 1091*w*, 1046*w*, 1017*w*, 868*w*. **G2-L** α_D: + 8.0 (c. 1.0, $CHCl_3$). **G2-D** α_D: – 6.5 (c. 1.0, $CHCl_3$).

3 CD Spectroscopy

All CD spectra were measured for 10 mM samples in methanol – absorbance spectra were recorded to ensure compounds or solvent were not too strongly absorbing. In all cases, they were not. It should be noted that the intensity of the CD spectra differ depending on the nature of the compound, the smallest CD bands were observed for the Boc-protected amino acids, in which case, some noise in the signal is visible. The largest spectra were observed for the target compounds – which may indicate a degree of self-assembly (which is known to enhance CD band intensity for chiral nanostructures).

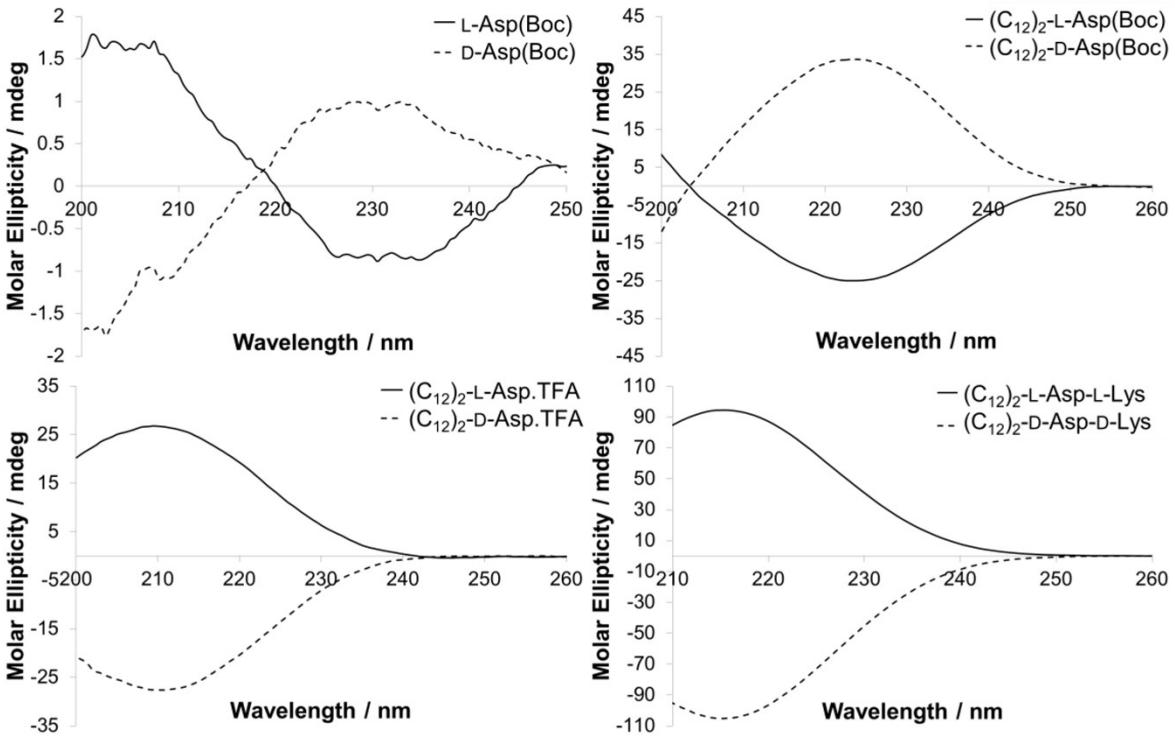

Figure S1. CD spectra of Boc-protected aspartic acid starting materials (top left); **1-L** and **1-D** (top right), **2-L** and **2-D** (bottom left) and **G1-L** and **G1-D** (bottom right). All samples are 10 mM in MeOH.

4 Assay Methods and Data

Nile Red Encapsulation Assay. The binder (100 μM) was dissolved in phosphate buffered saline (PBS, 0.01 M, endowed with NaCl (138 mM) and KCl (2.7 μM)). In a cuvette, an aliquot of this solution was diluted by addition of PBS to a total volume of 1 mL before Nile red (1 μL, 2.5 mM in ethanol) was added. Following inversion to ensure mixing, fluorescence intensity at 635 nm was recorded using a 550 nm excitation wavelength.

Dynamic Light Scattering and Zeta Potential. Aggregate characteristics were determined using a Zetasizer Nano (Malvern Instruments Ltd., Worcestershire, UK), based on the principle of measurement of the backscattered light fluctuations at an angle of 173° and the calculation of an autocorrelation function. Data were recorded from 15–20 runs per single measurement, each of which was carried out at 25°C using folded capillary cells (DTS 1060). Monomer solutions were freshly prepared by dissolving an appropriate amount of dry compound in filtered aqueous media (e.g. 10 mM Tris HCl, 150 mM NaCl). All samples were agitated and incubated at 25°C for 10 minutes prior to measurement. Data are reported based on volume distribution.

Heparin Binding Assay – in Buffer. A cuvette containing 2 mL of MalB (25 μM), heparin (27 μM) and NaCl (150 mM) in Tris HCl (10 mM) was titrated with binder stock solution to give the cuvette a suitable binder-heparin charge ratio. The binder stock solution was composed of the original MalB/heparin/NaCl/Tris HCl stock solution endowed additionally with a concentration of binder such that, after addition of 10 μL binder stock, the cuvette charge ratio (+:–) is 0.037. After each addition, the cuvette was inverted to ensure good mixing and the absorbance at 615 nm was recorded against a Tris HCl (10 mM) baseline. Absorbance was normalised between a solution of MalB (25 μM), NaCl (150 mM) in Tris HCl (10 mM) and one containing MalB (25 μM), heparin (27 μM), NaCl (150 mM) in Tris HCl (10 mM).

Heparin Binding Assay – in Serum. Fourteen cuvettes were charged with 1.75 mL of MalB (28.53 μM) in Tris HCl (10 mM) and a volume of binder stock solution to give the cuvette a suitable binder-heparin charge ratio. The binder stock solution was additionally endowed with its own MalB (25 μM), heparin (27 μM) and Tris HCl (10 mM) concentrations. The concentration of binder in the binder stock was determined in the same manner described for the heparin displacement assay in buffer. Separately, a heparin (216 μM) solution was made in

100% human serum. Sequentially, each cuvette was titrated with 0.25 mL of the heparin-in-serum solution and inverted to ensure thorough mixing. The absorbance was recorded at 615 nm against a baseline of (1.75 mL 10 mM Tris HCl, 0.25 mL 100% Human Serum) and a normalisation range for absorption was set against a solution containing exclusively MalB (25 μM) and one containing MalB (25 μM) and heparin (27 μM).

5 Transmission Electron Microscopy

Transmission Electron Microscopy. Solutions were prepared in clean water at concentrations above previously-calculated CMC values to ensure compounds were present in their assembled form. It was not possible to obtain TEM images in buffer or serum as crystallised salts and/or proteins dominate the image on drying from such samples. Heparin was introduced at a charge ratio (+:–) under which the binder was known to exhibit significant interaction with it. Once prepared, aliquots of each solution were loaded on a formvar grid, negatively stained with uranyl acetate and allowed to dry before imaging.

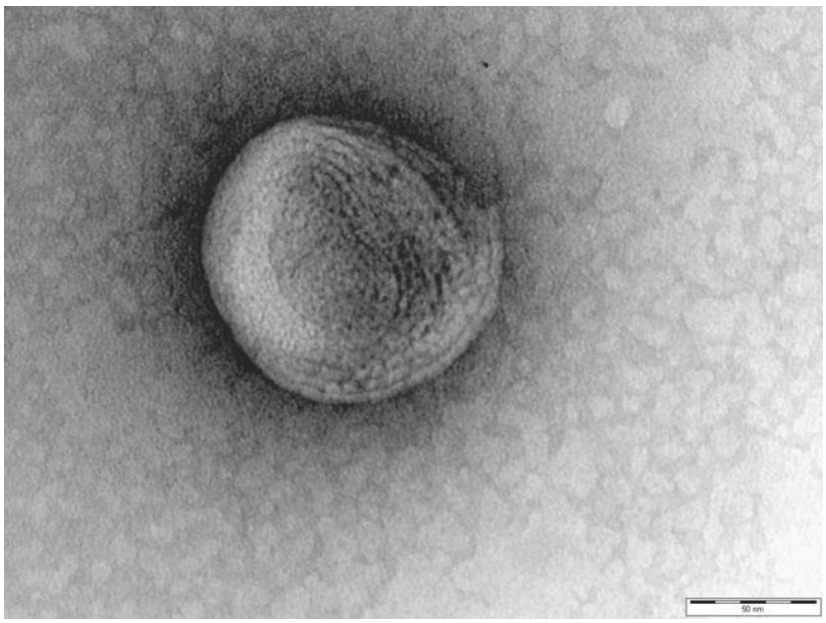

Figure S2. TEM image of **G1-D**, scale bar = 50 nm. On drying, the system forms a multi-layer system – this may be a series of worm-like micelles, or could be a multi-lamellar vesicle type system (see modelling below which investigates drying effects on morphology).

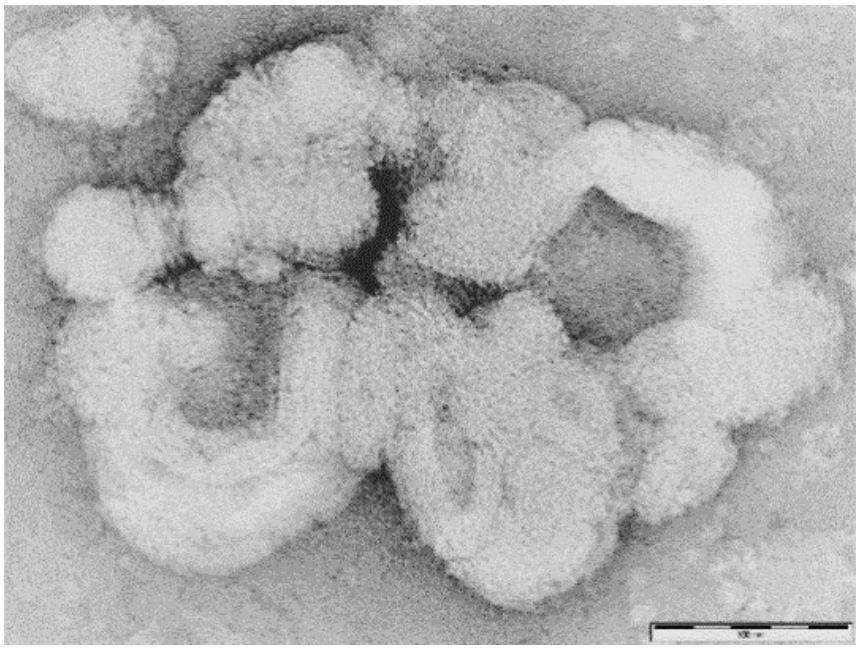

Figure S3. TEM image of worm-like micelles of **G1-L** bound to heparin, scale bar = 100 nm. On drying, the worm-like micelle-heparin complex hierarchically assembles into larger aggregates. Worm like micelles can most clearly be visualised curved into 'U shapes' in the lower aggregates – multiple cylindrical micelles appear to be packed together in these regions – we propose via a hierarchical assembly process such as that reported previously.[1]

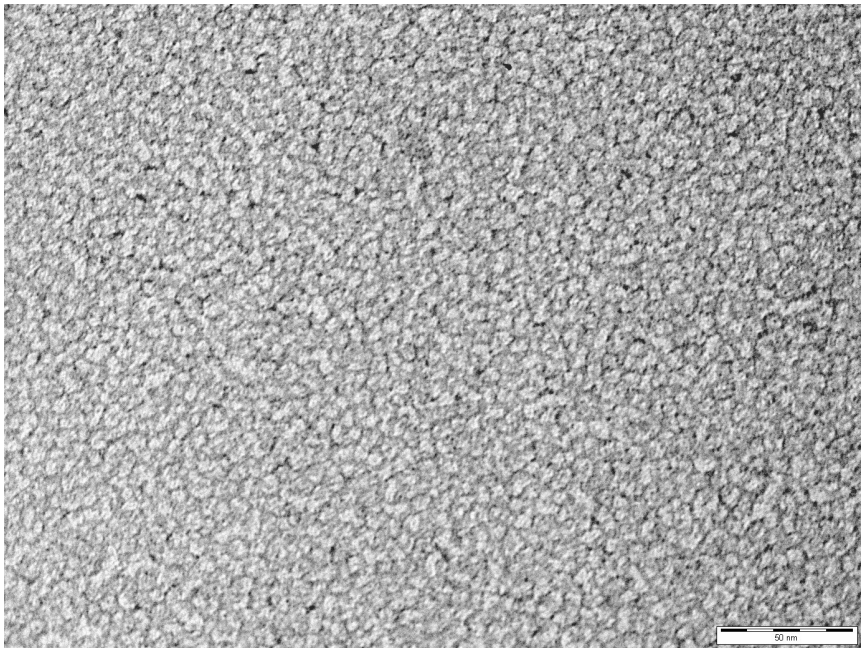

Figure S4. TEM image of **G2-L** showing the formation of spherical miceelles, scale bar = 50 nm.

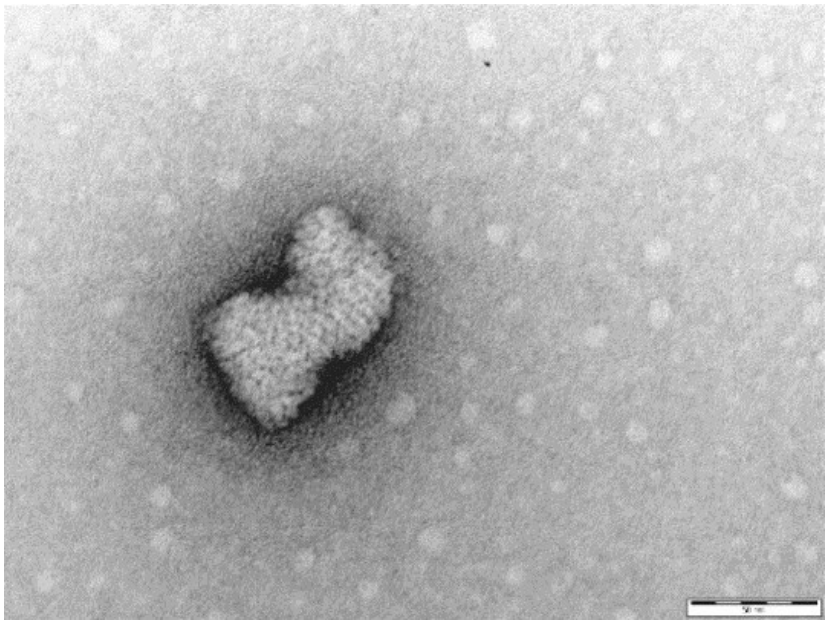

Figure S5. TEM image of spherical micelles of **G2-L** bound to heparin, scale bar = 50 nm. Some free micelles can be seen within the image, but most have further aggregated hierarchically on binding to heparin and drying to yield a nanostructure which in this case is ca. 50 nm in diameter. This hierarchical aggregation process has been characterised in detail by us previously for related systems.[1]

6 Degradation Assay and MS Data

The binder was dissolved (200 μM) in ammonium carbonate (10 mM, pH 7.5). 250 μL of this binder solution was combined with 250 μL of a Gly-Ala standard (1 mM, in 10 mM ammonium carbonate) for mass spectrometric analysis. Following incubation of the binder solution for 24 hours at 37^{o}C, the same analysis was repeated. The individual spectra of the binder sample at 0 hours, 4 hours, 7 hours and 24 hours highlighting the loss of molecular ion against standard are shown in Figures S6 and S7.

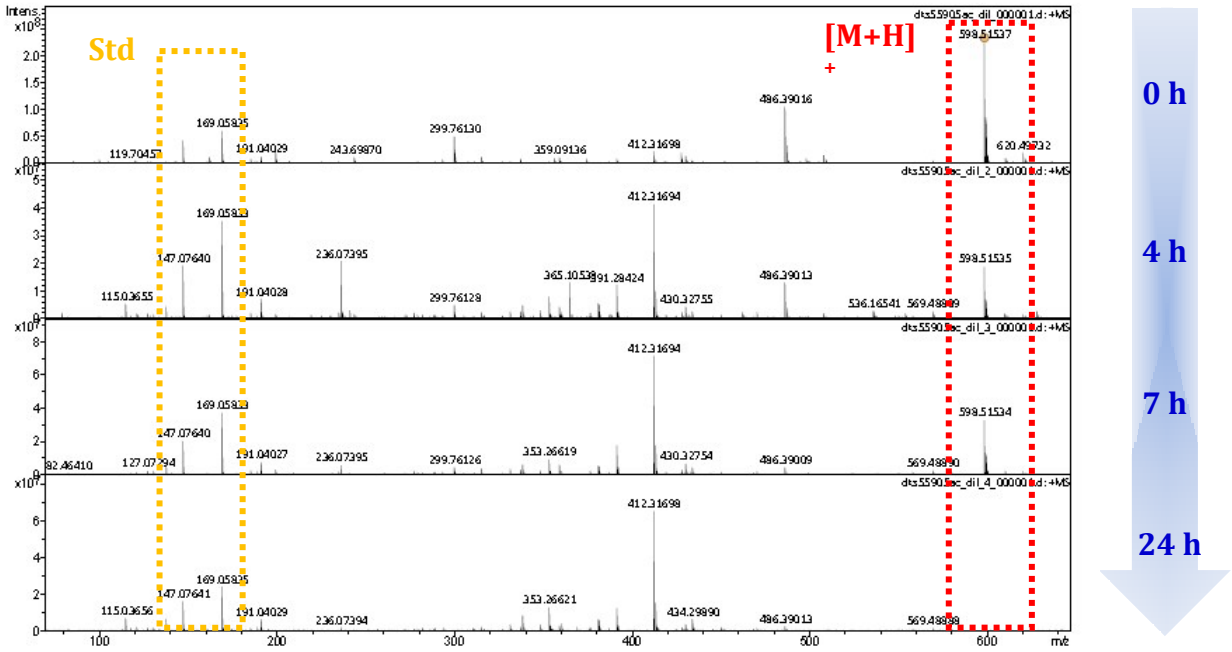

Figure S6. MS degradation assay of **G1-L**.

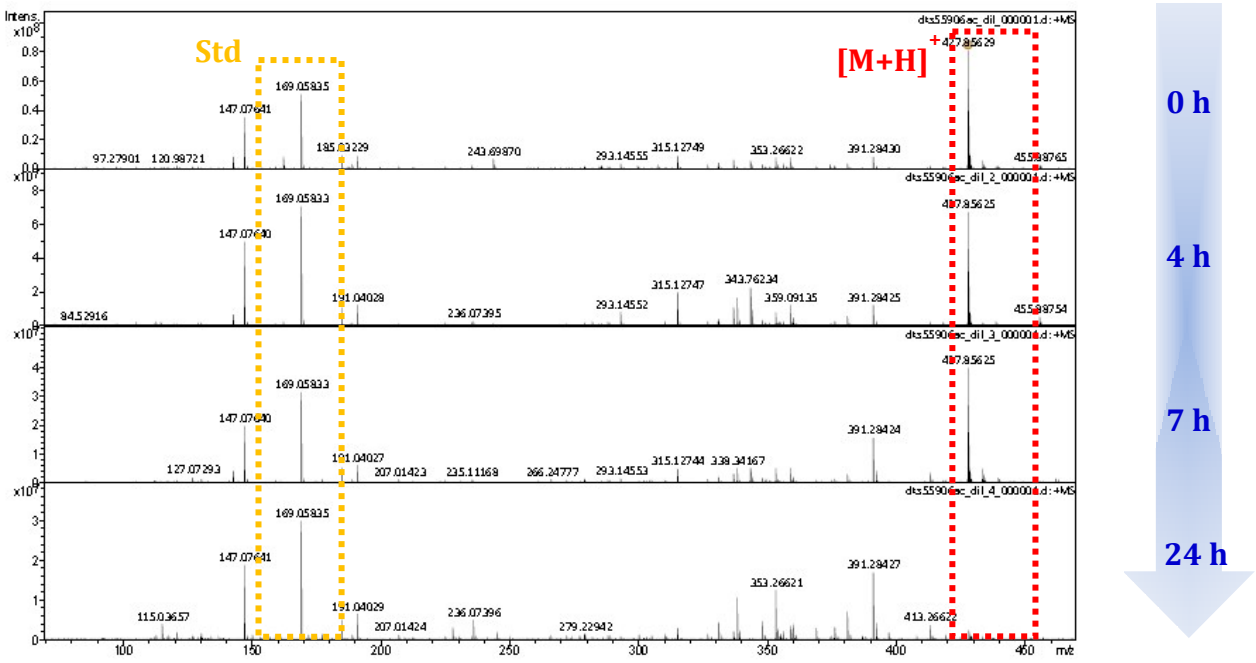

Figure S7. MS degradation assay of **G2-L**.

7 ITC Methods and Data Analysis

ITC experiments were performed with a MicroCal PEAQ-ITC calorimeter (Malvern, UK) at 25°C. The cell volume was 280 μL. All experiments were conducted in a forward manner, that

is, by step-by-step injections of a constant volume of concentrated $\mathbf{G_1}$ and $\mathbf{G_2}$ SAMul solutions into the calorimetric cell containing buffer (Tris HCl 10 mM/150 mM NaCl), or buffered solutions of heparin, respectively. Specifically, for CMC determination, a constant 1 μL portion of each SAMul solutions (1 mM for $\mathbf{G_1}$ and 250 μM for $\mathbf{G_2}$) were injected 37 times into the reaction cell at 210 s intervals. For heparin binding, a series of SAMul solutions (18 mM for $\mathbf{G_1}$ and 4 mM for $\mathbf{G_2}$) were injected in 37 portions of 1 μL at 210 s intervals. The polyanion concentration on the calorimeter cell was 5.2 mM and 1.2 mM for $\mathbf{G_1}$ and $\mathbf{G_2}$, respectively, such that the concentration of **G1** and **G2** was always above the CMC, and allowing us to make the assumption that the micelles remained intact throughout the experiment. All solutions and buffer were degassed for 30 min at room temperature under stirring at 500 rpm prior to each experiment. After careful washing, the cell was pre-rinsed with a portion of the buffer or heparin solutions, respectively. Upon filling cell and syringe, stirring was turned and each system was allowed to thermally equilibrate for 30 minutes.

During heparin/SAMul binding experiments, when all binding sites were occupied, only a heat signal resulting from mixing, dilution effects and liquid friction was observed. The values of these unspecific heats were further confirmed by control experiments (data not shown); accordingly, they were subtracted from the relevant data set to yield the corrected integrated data of Figure 3. All experiments were run in triplicate.

SAMul CMC determination via ITC

Figure S8 shows the demicellization thermogram of compounds **G2** in buffer solution as an example. The injection of the concentrated SAMul solution into the buffer mostly resulted in large, endothermic signals, followed by a series of small, exothermic peaks in the latest stages of the experiment (Figure S8A, insert). The enthalpy change characterizing the first part of the thermogram, corresponding to the addition of the SAMul stock solution (which, for each system, was always higher than the corresponding CMC) to the buffer, is due to demicellization, micelle dilution, and dilution of the surfactant monomers. In the final part of the thermogram, the further addition of a concentrated SAMul micellar solution to the sample cell leads to heat effects due to micellar dilution, being the SAMul concentration in the cell well above the corresponding CMC. Subtraction of the micelle dilution heat, normalization per mol of SAMul,

and integration of the heat raw data yielded the observed heat Q as a function of SAMul concentration C, as shown in panels Figure S8A.

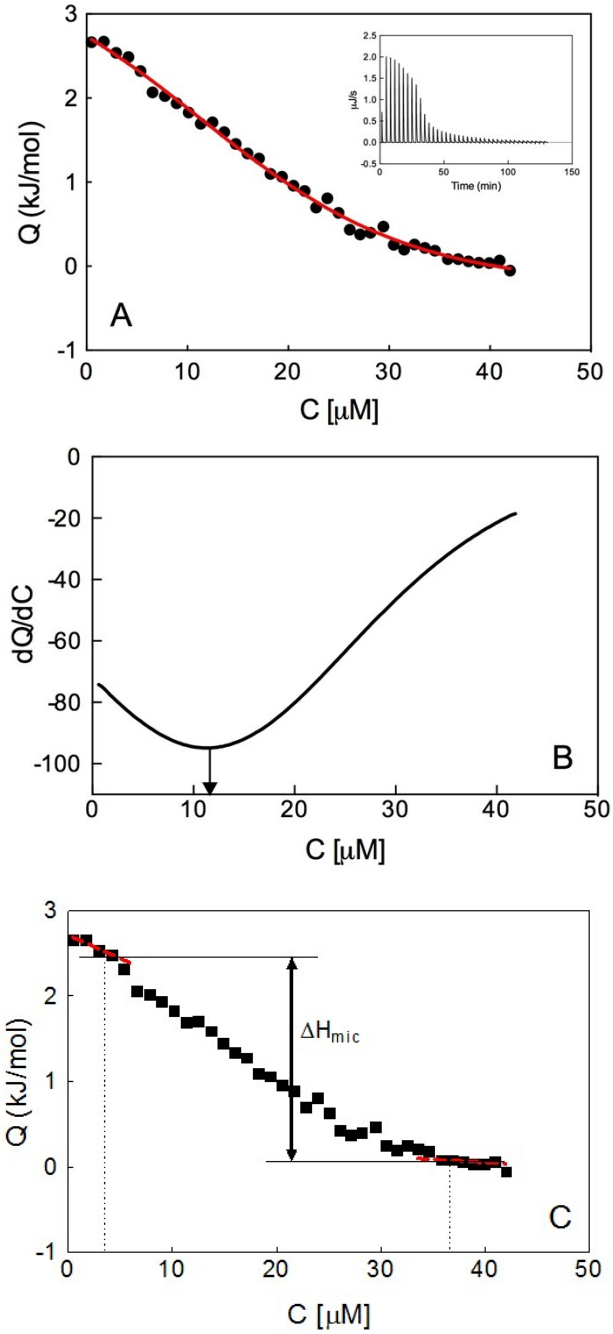

Figure S8. ITC demicellization of SAMul compound **G2** in Tris HCl 10mM/150 mM NaCl at 25°C. (A) Heat observed on each injection vs. final **G2** concentration in the calorimetric cell. Symbols: experimental data; red line: Boltzmann fit ($R^2 = 0.9953$). Insert: Measured heat power vs. time elapsed during the titration. (B) The first derivative of the curve in A (in arbitrary units). The CMC is taken as the x-value at the minimum of dQ/dC curve (indicated by the arrow). (C) Determination of the ΔH_{mic} obtained from the integrated ITC data.

The CMC is defined as the midpoint of the Q vs. C curve in Figures S8A. For a precise determination of the midpoint of the demicellization process, first Q vs C data were fitted to a suitable model and then the first derivative of the Q vs C fitting curve was calculated (Figure S8B). The CMC corresponds to the minimum of the derivative curve, as highlighted by the arrow in Figure S8B. From the ITC titration curve, the ΔH_{mic} is calculated from the enthalpy difference of the two levels of the titration curve as shown in Figure S8C. The experimental determination of the ΔH_{mic} and the CMC values allowed the calculation of other thermodynamics parameters. The free energy of micellization (ΔG_{mic}) is given by the expression $\Delta G_{mic} = RT \ln CMC'$, where R is the gas constant (8.31×10^{-3} kJ/mol K) and T is the absolute temperature, and CMC' is the critical micellization concentration expressed in molar fraction. The change in entropy associated with the micellization ($T\Delta S_{mic}$) can be calculated from the second law of thermodynamics by using the Gibbs–Helmholtz equation $T\Delta S_{mic} = \Delta H_{mic} - \Delta G_{mic}$. All the thermodynamic parameters of micellization for both SAMul systems are listed in Table S1.

Table S1. ITC-derived thermodynamics of micellization for SAMul **G1** and **G2**.

	ΔH_{mic} (kJmol^{-1})	ΔG_{mic} (kJmol^{-1})	$T\Delta S_{mic}$ (kJmol^{-1})
G1	-3.58	-34.13	+30.55
G2	-2.40	-38.03	+35.63

From the comparison of the values of both ΔH_{mic} and $T\Delta S_{mic}$ reported in Table S1, it can be seen that the major driving force for micelle formation is hydrophobic interactions for both wormlike (**G1**) and spherical (**G2**) micelles. Specifically, the entropy contribution dominates the micellization process in buffered solutions, with the enthalpy playing a minor role ($|T\Delta S_{mic}| >> |\Delta H_{mic}|$). This is specifically related to the releasing of the water molecules in hydration shells around the hydrophobic parts of the SAMul monomeric units with the subsequent production of hydrophobic forces. The entropy of formation of spherical micelles from **G2** is greater than that of worm-like micelles from **G1** because each small spherical micelle contains far fewer molecules, and hence they are much greater in number.

8 Multiscale Modeling Methods

Fundamentals of Dissipative Particle Dynamics (DPD) Theory

DPD[2] is a particle-based mesoscopic simulation technique effectively employed to investigate phenomena like self-assembling behaviour of surfactants[3,4] or block copolymers in melt and in solution,[5-7] as well as complex amphiphilic micelles.[8-11]

In a DPD simulation, the actual material is modelled as a collection of spherical particles (called *beads*), each representing a group of small molecules or extensive molecular fragments, which interact by pairwise additive forces expressed by a conservative, dissipative, and random potential. The overall force acting on a bead i can be expressed as $\boldsymbol{F}_i = \sum_{j \neq i} (\boldsymbol{F}_{ij}^C + \boldsymbol{F}_{ij}^D + \boldsymbol{F}_{ij}^R)$ and is calculated by summation over all other particles within a certain cuto radius, r_c, which represents the intrinsic length scale of the DPD model.

The conservative force represents the excluded volume interactions between particles i and j in the dimensionless form $\boldsymbol{F}_{ij}^C = a_{ij} (1 - r_{ij}) \hat{\boldsymbol{r}}_{ij}$, where $\boldsymbol{r}_{ij} = \boldsymbol{r}_i - \boldsymbol{r}_j$, $r_{ij} = |\boldsymbol{r}_{ij}|$, $\hat{\boldsymbol{r}}_{ij} = \boldsymbol{r}_{ij}/r_{ij}$, a_{ij} is the maximum repulsion between particles i and j. The dissipative ($\boldsymbol{F}_{ij}^D = -\gamma\, \omega(r_{ij})^2 (\hat{\boldsymbol{r}}_{ij} \cdot \boldsymbol{v}_{ij}) \hat{\boldsymbol{r}}_{ij}$) and random ($\boldsymbol{F}_{ij}^R = \sigma\, \omega(r_{ij})\, \hat{\boldsymbol{r}}_{ij}\, \zeta/(\Delta t)^{-1/2}$) forces act as heat sink and source, respectively, and the combined effect of the two forces performs as a thermostat, where γ is a friction coe cient related to the thermal noise amplitude σ via the fluctuation−dissipation theorem, $\sigma^2 = 2\gamma k_B T$. $\omega(r)$ is a weight function, ζ is a normally distributed random variable with zero mean and unit variance that is uncorrelated for di erent particle pairs, Δt is the time step of an integration scheme, and $\boldsymbol{v}_{ij} = \boldsymbol{v}_i - \boldsymbol{v}_j$ is the relative velocity of the i^{th} and the j^{th} particles. The equations of particle motion, $d\boldsymbol{r}_i/dt = \boldsymbol{v}_i$ and $d\boldsymbol{v}_i/dt = \boldsymbol{F}_i$, are solved using as integration scheme the velocity-Verlet algorithm.

When modelling polymer chains or complex molecules, typically two additional forces are acting between bonded beads: a harmonic spring connecting two adjacent particles i and j: $\boldsymbol{F}_{ij}^B = k_b(r_{ij} - r_0) \hat{\boldsymbol{r}}_{ij}$, where k_b is a spring constant and r_0 the equilibrium distance between the particles, and $\boldsymbol{F}_{ijz}^A = 1/2\, k_\theta \sin(\theta_0 - \theta_0)$, where k_θ is a spring constant and θ_0 the equilibrium angle between adjacent beads triples ijz in a row.

Derivation of the Mesoscale Models

The first necessary step of a coarse-grain (CG) calculation is the construction of the required CG models. This is usually performed taking into account the relevant structural /thermodynamic properties of the molecules under investigation and matching them with the corresponding atomistic features in order to assure the ability of the CG simulation of reproducing them. Accordingly, in this work **G1** and **G2** CG models were derived by a direct comparison of the appropriate atomistic and DPD pair-pair correlation functions, according to a procedure validated by our group on other related self-assembling compounds.[12-16] The obtained models together with the related bead types are displayed in Figure S9.

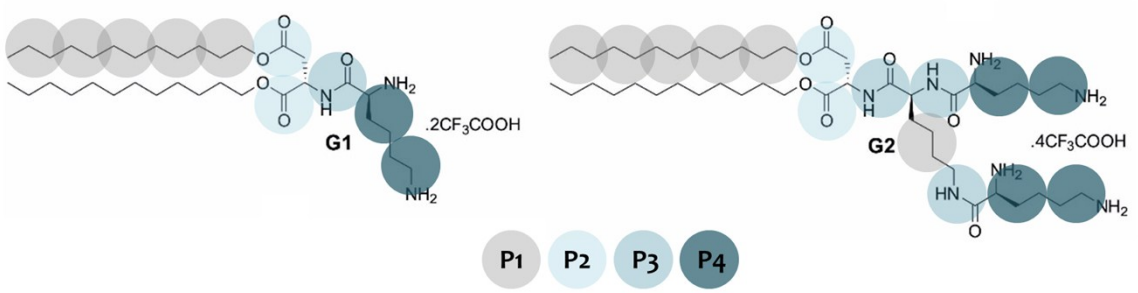

Figure S9. Schematic representation of the CG models of **G1** and **G2** compounds.

Solvent molecules were simulated by single bead types W, and an appropriate number of counterions of a charge of ± 1 were added to account for the experimental ionic strength.

As mentioned above, in DPD intra- and intermolecular interactions between particles are expressed by the conservative force $\boldsymbol{F}_{ij}^{C}$, whose intensity is proportional to the pair-repulsive parameter a_{ij}, which accounts for the underlying chemistry of the system considered. In this work, we correlated the interaction energies estimated from atomistic molecular dynamics (MD) simulations to the mesoscale a_{ij} parameter values as proposed for other self-assembling compounds.[1,9,12,13,17] Following this computational recipe reported briefly in the following paragraphs, **G1**/**G2** compound models were built and geometry optimized. A suitable number of molecules for each compound were then solvated in a TIP3P water box to generate a bulk system with concentration lower than the corresponding experimental CAC value. Then, the required amount of Na^+ and Cl^- ions were added to neutralize the system and to mimic an ionic strength of 150 mM, removing eventual overlapping water molecules. The solvated molecules were subjected to a combination of steepest descent/conjugate gradient minimisation of the

potential energy, during which all bad contacts were relieved. The relaxed systems were then gradually heated to 300 K in three intervals by running constant volume-constant temperature (NVT) molecular dynamics (MD) simulation, allowing a 0.5 ns interval per each 100 K. Subsequently, 10 ns MD simulations under isobaric-isothermal (NPT) conditions were conducted to fully equilibrate each solvated **G1**/**G2** system. The SHAKE algorithm with a geometrical tolerance of 5×10^{-4} Å was imposed on all covalent bond involving hydrogen atoms. Temperature control was achieved using the Langevin temperature equilibration scheme and an integration time step of 2 fs. At this point, these MD runs were followed by other 10 ns of NVT MD data collection runs, necessary for the estimation of the interaction energies. The Particle Mesh Ewald technique was used to treat the system electrostatics. The interaction energies between the system molecular constituents were estimated using the Molecular Mechanics/Poisson-Boltzmann Surface Area (MM/PBSA) methodology[18] on a single MD production trajectory of each model. All MD simulations were carried out using the AMBER 14[19] platform running on our CPU/GPU hybrid cluster and applying the *ff14SB* and the *gaff* force field.[20]

Once obtained, the atomistic interaction energies were rescaled onto the corresponding mesoscale segments adapting the procedure described in detail in reference 17. To accomplish this task, two reference values have to be selected. The self-repulsive interaction parameter for water a_{WW} was set equal to 25 k_BT/r_c to fit the isothermal compressibility of water at a dimensionless bead density ρ of 3.[1] At the same time, the hydrophobic force was captured by setting the interaction parameter a_{ij} between the water bead W and the alkyl tail bead C as 80 k_BT/r_c. The counterions were set to have the interaction parameters of water.[21] Accordingly, the conservative DPD interaction parameters a_{ij} (in units of k_BT/r_c) are the following: a_{P1_P1}=27, a_{P2_P1}=58, a_{P2_P2}=29, a_{P3_P1}=50, a_{P3_P2}=27, a_{P3_P3}=30, a_{P4_P1}=76, a_{P4_P2}=51, a_{P4_P3}=50, a_{P4_P4}=41, a_{W_P1}=80, $a_{W\text{-}P2}$=34, a_{W_P3}=32, a_{W_P4}=23.

Simulation Details

DPD simulations of **G1** and **G2** self-assembling in solution were performed in 3D-periodic cubic boxes of 30^3 r_c^3. The proper number of molecules was added to the simulation box in order to fit experimental relevant concentrations. Simulations were carried out with a time step of Δt = 0.04 $(k_BT/m)^{-1/2}r_c$ and a simulation period of 4×10^5 steps or longer until stable morphology was observed.

Drying Effects on Morphology

We acknowledge the limitations of TEM as an imaging methodology for nanoscale morphologies – and hence, in our pursuit to investigate the effect of solvent evaporation occurring during sample preparation for TEM analysis, we simulated **G1**/**G2** self-organization during solvent evaporation at mesoscale level. The effect of solvent evaporation was reproduced in the DPD framework according to the procedure originally proposed by Neratova et al.[22] for diblock copolymers and extended by our group[23] to self-assembling of amphiphilic micelles[16]. Briefly, the **G1/G2** solution obtained from bulk simulation was placed on an impenetrable, fixed, non-interacting substrate. At the top of the film phase, a gas phase and an exchange phase were created. During the virtual evaporation, when solvent particles leave the film phase and enter into the exchange region, they are transformed into gas particles. As a result of such process, the fraction of the gas phase increases, and the thickness of the film decreases. Gas and film phases were assumed to be immiscible.

Simulations were carried out in a box of $30r_c \times 30r_c \times 60r_c$ with a time step of $\Delta t = 0.03\ (k_BT/m)^{-1/2}r_c$ until stabilization occurred (approx. 7×10^5 simulation steps). In all DPD studies the following reduced units were used: r_c is the unit of length, m is the mass of a DPD particle, and k_BT is the unit of energy.

We observed that as **G1** was dried onto a surface (Fig. S10) the cylindrical micellar morphology evolved and formed lamellar structures, as a result of surface-level interactions and general desolvation effects. This kind of process was observed in the TEM images of **G1** (see Fig. S2) which showed some evidence of a multi-lamellar morphology. Conversely, for **G2** the spherical micelles observed in solution are largely retained on drying down onto a surface (Fig. S11) – once again, this is consistent with the evidence observed by TEM (Fig. S4).

In the presence of heparin, cylinders and micelles can be more clearly observed for G1 and G2 respectively by TEM (Figs. S3 and S5). We reason that the hierarchical assembly process, which occurs on heparin binding, limits the evolution of the nanoscale morphologies on drying, and hence allows them to be more easily visualised.

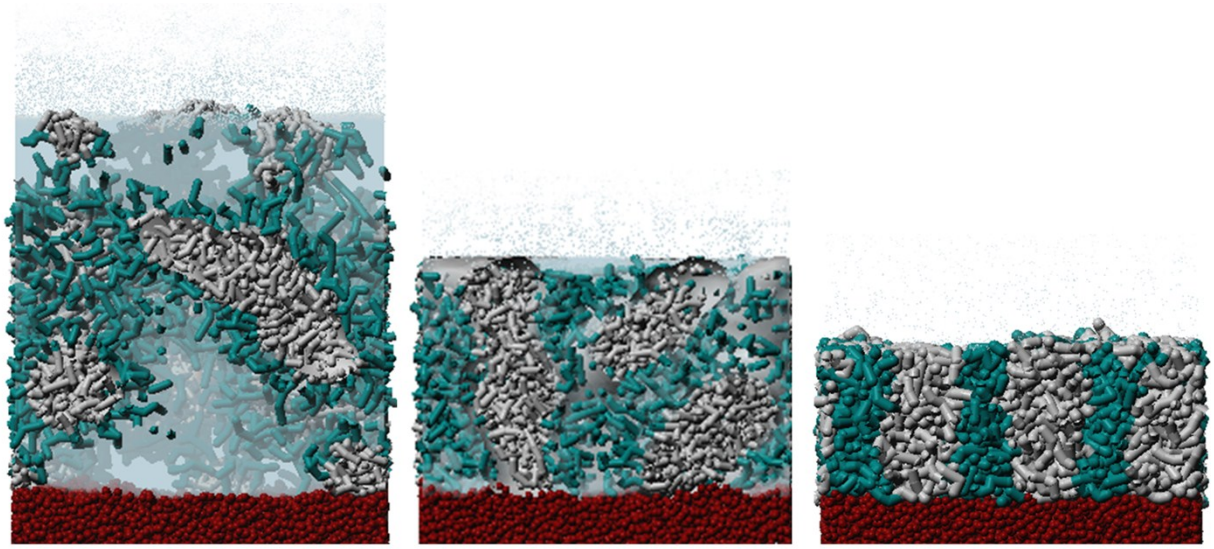

Figure S10. Snapshots taken at different increasing time (from left to right) during virtual solvent evaporation from **G1** solution. The hydrophobic core is portrayed as grey sticks, while the hydrophilic shell is colored in forest green. Substrate and solvent are depicted in brown and light blue, respectively.

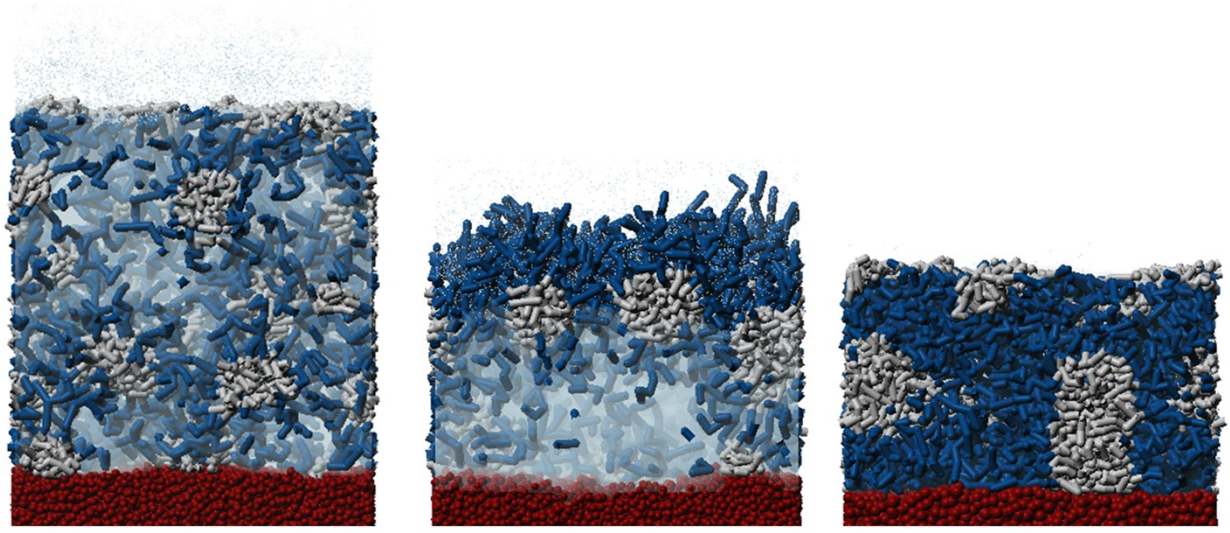

Figure S11. Snapshots taken at different increasing time (from left to right) during virtual solvent evaporation from **G2** solution. The hydrophobic core is portrayed as grey sticks, while the hydrophilic shell is colored in blue. Substrate and solvent are depicted in brown and light blue, respectively.

9 References

1 V. M. P. Vieira, V. Liljeström, P. Posocco, E. Laurini, S. Pricl, M. A. Kostiainen and D. K. Smith, *J. Mater. Chem. B*, 2017, **5**, 341-347.

2 R. D. Groot and P. B. Warren, *J. Chem. Phys.* 1997, **107**, 4423.

3 P. Posocco, A. Perazzo, V. Preziosi, E. Laurini, S. Pricl and S. Guido, *RSC Adv.* 2016, **6**, 4723.

4 L. Rekvig, M. Kranenburg, J. Vreede, B. Hafskjold and B. Smit, *Langmuir* 2003, **19**, 8195.

5 P. Posocco, M. Fermeglia and S. Pricl, *J. Mater. Chem.* 2010, **20**, 7742.

6 Z. Posel, P. Posocco, M. Fermeglia, M. Lisal and S. Pricl, *Soft Matter* 2013, **9**, 2936.

7 O. A. Guskova and C. Seidel, *Macromolecules* 2011, **44**, 671.

8 Z. Posel, Z. Limpouchová, K. Šindelka, M. Lísal and K. Procházka, *Macromolecules* 2014, **47**, 2503.

9 A. Barnard, P. Posocco, M. Fermeglia, A. Tschiche, M. Calderon, S. Pricl and D. K. Smith, *Org. Biomol. Chem.* 2014, **12**, 446.

10 S. M. Bromfield, P. Posocco, C. W. Chan, M. Calderon, S. R. Guimond, J. E. Turnbull, S. Pricl and D. K. Smith, *Chem. Sci.* 2014, **5**, 1484.

11 C. Chen, P. Posocco, X. Liu, Q. Cheng, E. Laurini, J. Zhou, C. Liu, Y. Wang, J. Tang, V. D. Col, T. Yu, S. Giorgio, M. Fermeglia, F. Qu, Z. Liang, J. J. Rossi, M. Liu, P. Rocchi, S. Pricl and L. Peng, *Small* 2016, **12**, 3667.

12 X. Liu, J. Zhou, T. Yu, C. Chen, Q. Cheng, K. Sengupta, Y. Huang, H. Li, C. Liu, Y. Wang, P. Posocco, M. Wang, Q. Cui, S. Giorgio, M. Fermeglia, F. Qu, S. Pricl, Y. Shi, Z. Liang, P. Rocchi, J. J. Rossi and L. Peng, *Angew. Chem. Int. Ed.* 2014, **53**, 11822.

13 D. J. Welsh, P. Posocco, S. Pricl and D. K. Smith, *Org. Biomol. Chem.* 2013, **11**, 3177.

14 X. Liu, J. Wu, M. Yammine, J. Zhou, P. Posocco, S. Viel, C. Liu, F. Ziarelli, M. Fermeglia, S. Pricl, G. Victorero, C. Nguyen, P. Erbacher, J.-P. Behr and L. Peng, *Bioconjugate Chem.* 2011, **22**, 2461.

15 P. Posocco, S. Pricl, S. Jones, A. Barnard and D. K. Smith, *Chem. Sci.* 2010, **1**, 393.

16 T. Wei, C. Chen, J. Liu, C. Liu, P. Posocco, X. Liu, Q. Cheng, S. Huo, Z. Liang, M. Fermeglia, S. Pricl, X.-J. Liang, P. Rocchi and L. Peng, *Proc. Natl. Acad. Sci. USA* 2015, **112**, 2978.

17 G. Scocchi, P. Posocco, M. Fermeglia and S. Pricl, *J. Phys. Chem. B* 2007, **111**, 2143.

18 V. Tsui and D. A. Case, *Biopolymers* 2000, **56**, 275.

19 D. A. Case, V. Babin, J. T. Berryman, R. M. Betz, Q. Cai, D. S. Cerutti, T. E. Cheatham, T. A. I. Darden, R. E. Duke, H. Gohlke, A. W. Goetz, S. Gusarov, N. Homeyer, P. Janowski, J. Kaus, I. Kolossváry, A. Kovalenko, T. S. Lee, S. LeGrand, T. Luchko, R. Luo, B. Madej, K. M. Merz, F. Paesani, D. R. Roe, A. Roitberg, C. Sagui, R. Salomon-Ferrer, G. Seabra, C. L. Simmerling, W. Smith, J. Swails, R. C. Walker, J. Wang, R. M. Wolf, X. Wu and P. A. Kollman, *AMBER 14, University of California, San Francisco* 2014.

20 Y. Duan, C. Wu, S. Chowdhury, M. C. Lee, G. Xiong, W. Zhang, R. Yang, P. Cieplak, R. Luo, T. Lee, J. Caldwell, J. Wang and P. Kollman, *J. Comput. Chem.* 2003, **24**, 1999.

21 X. N. Fan, S. Phan-Thien, X. W. Chen and T. Y. Ng *Phys. Fluids* 2006, **18**, 63102.